

# Excitation–Emission Spectra and Fluorescence Quantum Yields for Fresh and Aged Biogenic Secondary Organic Aerosols

Hyun Ji (Julie) Lee,<sup>†</sup> Alexander Laskin,<sup>‡</sup> Julia Laskin,<sup>§</sup> and Sergey A. Nizkorodov<sup>\*,†</sup>

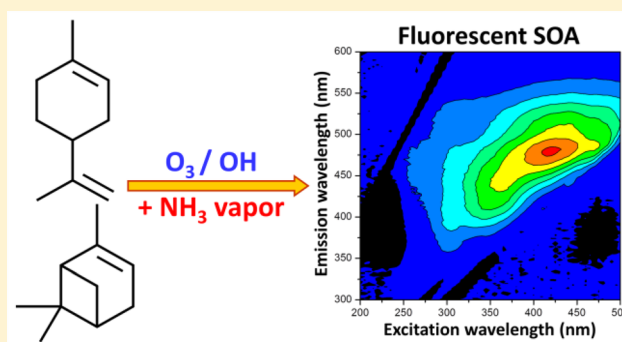
<sup>†</sup>Department of Chemistry, University of California, Irvine, California 92697, United States

<sup>‡</sup>Environmental Molecular Sciences Laboratory, Pacific Northwest National Laboratory, Richland, Washington 99352, United States

<sup>§</sup>Physical Sciences Division, Pacific Northwest National Laboratory, Richland, Washington 99352, United States

## S Supporting Information

**ABSTRACT:** Certain biogenic secondary organic aerosols (SOA) become absorbent and fluorescent when exposed to reduced nitrogen compounds such as ammonia, amines, and their salts. Fluorescent SOA may potentially be mistaken for biological particles by detection methods relying on fluorescence. This work quantifies the spectral distribution and effective quantum yields of fluorescence of water-soluble SOA generated from two monoterpenes, limonene and  $\alpha$ -pinene, and two different oxidants, ozone ( $O_3$ ) and hydroxyl radical (OH). The SOA was generated in a smog chamber, collected on substrates, and aged by exposure to  $\sim 100$  ppb ammonia in air saturated with water vapor. Absorption and excitation–emission matrix (EEM) spectra of aqueous extracts of aged and control SOA samples were measured, and the effective absorption coefficients and fluorescence quantum yields ( $\sim 0.005$  for 349 nm excitation) were determined from the data. The strongest fluorescence for the limonene-derived SOA was observed for  $\lambda_{\text{excitation}} = 420 \pm 50$  nm and  $\lambda_{\text{emission}} = 475 \pm 38$  nm. The window of the strongest fluorescence shifted to  $\lambda_{\text{excitation}} = 320 \pm 25$  nm and  $\lambda_{\text{emission}} = 425 \pm 38$  nm for the  $\alpha$ -pinene-derived SOA. Both regions overlap with the EEM spectra of some of the fluorophores found in primary biological aerosols. Despite the low quantum yield, the aged SOA particles may have sufficient fluorescence intensities to interfere with the fluorescence detection of common bioaerosols.



## 1. INTRODUCTION

Primary biological aerosol particles (PBAP), also termed bioaerosols, are emitted directly from the biosphere to the atmosphere and include viruses (0.01–0.3  $\mu\text{m}$ ), bacteria (0.1–10  $\mu\text{m}$ ), fungal and fern spores (1–3  $\mu\text{m}$ ), plant pollen (5–100  $\mu\text{m}$ ), and fragments of plant and animal matter (5–100  $\mu\text{m}$ ).<sup>1</sup> PBAP can be transported over significant distances before they are removed from the air by dry or wet deposition.<sup>2</sup> The airborne dispersal and transport of PBAP have significant impact on public health, especially in the occupational environments.<sup>3</sup> PBAP can account for up to 30% of submicrometer particles in rural and forest air,<sup>1</sup> and therefore have a strong effect on the Earth's climate and hydrological cycles by acting as cloud condensation and ice nuclei.<sup>4–6</sup> In addition to the natural sources, important anthropogenic emissions of PBAP can result from industrial sources or from an intentional release of biological airborne agents of terrorism.

Fluorescence spectroscopy offers a rapid and sensitive way for quantitative and qualitative analysis of PBAP.<sup>1,7,8</sup> Furthermore, fluorescence methods are capable of detecting and recording emission spectra of *single particles* in real-time.<sup>9–20</sup> One of the potential issues in detection of PBAP is significant interference from nonbiological particles such as primary organic aerosol (POA), secondary organic aerosol

(SOA), soot, and dust.<sup>1</sup> For example, a recent fluorescence microscopy study of liquid–liquid phase separation in particles demonstrated strong fluorescence of biogenic SOA produced by the atmospheric oxidation of isoprene ( $C_5H_8$ ), monoterpenes ( $C_{10}H_{16}$ ), and other biogenic compounds.<sup>21</sup> Single particle fluorescence measurements in ambient air have shown that the most frequently detected particles are those containing aged terpenes.<sup>22</sup>

Fluorescent particles must contain significant amounts of organic compounds with large absorption coefficients and fluorescence quantum yields. Biogenic SOA are not normally regarded as strong absorbers of solar radiation.<sup>23</sup> However, recent studies have demonstrated that Maillard (browning) reactions of carbonyl compounds in biogenic SOA with reduced nitrogen compounds such as ammonia ( $NH_3$ ), ammonium ion ( $NH_4^+$ ), and amino acids significantly enhance the absorption coefficients of the SOA material<sup>24–27</sup> and make it more fluorescent.<sup>24</sup> Laskin et al.<sup>25</sup> observed a large number of highly conjugated, nitrogen-containing compounds in the aged

Received: February 8, 2013

Revised: May 5, 2013

Accepted: May 10, 2013

Published: May 10, 2013

limonene + O<sub>3</sub> SOA with high-resolution mass spectrometry. Nguyen et al.<sup>26</sup> found that the evaporation of the dissolved limonene + O<sub>3</sub> SOA material significantly accelerated the browning chemistry. Updyke et al. found that browning reactions occur in a wide range of both biogenic and anthropogenic SOA.<sup>27</sup> Similar browning effects have been observed during interactions of glyoxal and methyl glyoxal in aqueous solutions with ammonium sulfate and amino acids.<sup>28–37</sup> Finally, a number of other atmospheric processes such as oxidation of aromatics<sup>38</sup> can lead to the appearance of “brown carbon” – organic aerosol material that absorbs significantly in the UV and visible range.

While there is significant evidence of strong light absorption by the aged biogenic SOA, and more generally by the atmospheric “brown carbon”, quantitative measurements of their fluorescence spectra are currently lacking. In this work we present characteristic excitation–emission spectra and fluorescence quantum yields of freshly prepared and aged biogenic SOA from two monoterpenes, limonene and  $\alpha$ -pinene, and two oxidants, O<sub>3</sub> and OH. We find that both fresh and aged SOA exhibit fluorescence with an effective quantum yield of  $\sim 0.005$ . While aging has no significant effect on the fluorescence quantum yield, it increases the absorption by the SOA material and hence the fluorescence intensity. Comparison of the fluorescence properties of the SOA and other environmental fluorophores such as PBAP and Humic-Like Substances (HULIS) suggests that SOA particles may provide a sizable source of interference in the fluorescence-based PBAP detection. For example, if the mass concentration of SOA exceeds that of PBAP by more than an order of magnitude, the fluorescence from the SOA material may potentially be stronger than that from biological material. This effect may increase as the aerosol continues to age because of the increased photoabsorption by the aged aerosols.

## 2. EXPERIMENTAL SECTION

**2.1. Preparation and Aging of SOA.** SOA were prepared by oxidation of monoterpenes *d*-limonene (LIM) and  $\alpha$ -pinene (PIN) with ozone (O<sub>3</sub>) and hydroxyl radicals (OH) in a 5 m<sup>3</sup> Teflon chamber under low NO<sub>x</sub> conditions. We will refer to the four types of SOA samples studied in this work as LIM/O<sub>3</sub>, LIM/OH, PIN/O<sub>3</sub>, and PIN/OH. Each type of SOA was generated, aged, and characterized two to three times under identical conditions for reproducibility. Prior to each run, the chamber was purged overnight with 60 standard liters per minute (SLM) of clean air flow. NO and NO<sub>y</sub> concentrations in the chamber were monitored with a Thermo Scientific model 42i-Y NO<sub>y</sub> analyzer, and the O<sub>3</sub> concentration was monitored with a Thermo Scientific model 49i ozone analyzer. The particle size and number distribution was monitored with a TSI model 3936 scanning mobility particle sizer (SMPS). At the start of the reaction, the residual levels of particles, O<sub>3</sub> and NO<sub>y</sub> were below the detection level of the analyzers.

For the O<sub>3</sub> oxidation, approximately 600 ppb of O<sub>3</sub> was introduced into the chamber by flowing oxygen (99.994% purity) through a commercial ozone generator. Approximately 300 ppb of a precursor (LIM or PIN) was then added by injecting 10  $\mu$ L of the precursor into a glass trap and evaporating it fully with 4 SLM air flow. The chamber was mixed with a fan for a few minutes. Then, the fan was turned off in order to minimize the wall losses. The particle collection from the center of the chamber started after 30 min of dark reaction. For the OH oxidation, 40  $\mu$ L of 30% hydrogen

peroxide (by volume in water) was evaporated into the chamber resulting in  $\sim 2$  ppm of H<sub>2</sub>O<sub>2</sub>. The organic precursor mixing ratio was the same (300 ppb). After a brief period of mixing, 35 lamps (FS40T12/UVB, Solarc Systems Inc.) with emission centered at 310 nm were turned on to initiate the photooxidation. The steady-state OH concentration in this chamber was previously determined under similar conditions as  $\sim 2 \times 10^7$  molecules cm<sup>-3</sup> from the rate of isoprene decay.<sup>39</sup> The lights were turned off after two hours, and SOA was collected. All oxidation studies were carried out under low-NO<sub>x</sub> conditions, and therefore NO levels remained below detection levels (<1 ppb) while NO<sub>y</sub> levels remained constant (<3 ppb).

SOA were collected on two PTFE filters (Millipore 0.2  $\mu$ m pore size) in parallel at a constant flow rate of 10 SLM per filter. An activated carbon denuder (Sunset Laboratory) was installed between the chamber and the filters to help remove excess volatiles and O<sub>3</sub>. The amount of SOA collected on each filter was estimated from the SMPS data assuming an aerosol density of 1.2 g/cm<sup>3</sup> and 100% collection efficiency by the filters. The SOA filters were placed on top of polystyrene containers (5.5 cm diameter, 0.5 cm height), which were allowed to freely float on top of a 50 mL solution inside a larger polystyrene Petri dish (9.2 cm diameter, 1.5 cm height) as described in Updyke et al.<sup>27</sup> The solution for the sample was 0.1 M ammonium nitrate (NH<sub>4</sub>NO<sub>3</sub>), and that for the control was deionized water. The Petri dishes were covered and sealed with Parafilm tape. According to the AIM-II estimations,<sup>40</sup> the expected equilibrium gas-phase concentration of NH<sub>3</sub> in the  $\sim 50$  cm<sup>3</sup> head space volume was  $\sim 100$  ppb. The aging process lasted at least 72 h. We will refer to the aged and control SOA samples as aged-LIM/O<sub>3</sub>, control-LIM/O<sub>3</sub>, etc.

**2.2. Absorption and Fluorescence Spectra.** The aged and control SOA were extracted by sonicating the filter in 0.8 to 1.2 mL of deionized water for 10 to 15 min. The specific amount of water used in the extraction was chosen to achieve a 1.0 mg/mL (1000 ppm by weight) concentration of the dissolved SOA material. The completeness of the extraction of the SOA material by water was verified in our previous experiments;<sup>27</sup> we estimate that water extracted more than 90% of the organic material. For the absorption measurements, the extract was placed in an  $l = 1.0$  cm four-sided quartz cuvette (Starna Cells, Inc.). UV/vis absorption spectra were acquired using a single-beam spectrometer (Varian Cary 50 UV/vis Spectrophotometer) at a scan rate of 300 nm/min. A reference absorption spectrum of deionized water was taken in the same cuvette prior to any sample analysis. The base-10 absorption coefficient of the solution was calculated by dividing the base-10 absorbance of the SOA solution by the path length,  $\alpha_{\text{SOA}}(\lambda) = A(\lambda)/l$ .

Immediately following the absorption measurements, the cuvette was transferred into a Hitachi F-4500 instrument for fluorescence measurements. Emission spectra resulting from a single-wavelength excitation and the two-dimensional excitation–emission spectra were acquired at a scan rate of 1200 nm/min. For the emission spectra, a single wavelength (typically 349 nm) was chosen to excite the sample, and the emitted fluorescence was measured over the 300–600 nm range. For the excitation–emission spectra, the excitation wavelength varied over the 200–500 nm range in 5 nm steps, and the emitted fluorescence was recorded over the 300–600 nm range in 2 nm steps. The background for the fluorescence spectrum was deionized water for the SOA measurements and 0.05 M

sulfuric acid for the reference compound measurements (neither solution exhibited any detectable fluorescence).

The spectrum of the reference compound quinine sulfate (QS),  $(C_{20}H_{24}N_2O_2)_2 \cdot H_2SO_4 \cdot H_2O$ , dissolved in 0.05 M sulfuric acid was recorded immediately after the SOA spectra. QS is a convenient standard because of its high and wavelength-independent fluorescence quantum yield,  $QY_{QS} = 0.51$ .<sup>41–43</sup> The absorption spectrum of QS peaks at 349 nm (Figure 1(a)),

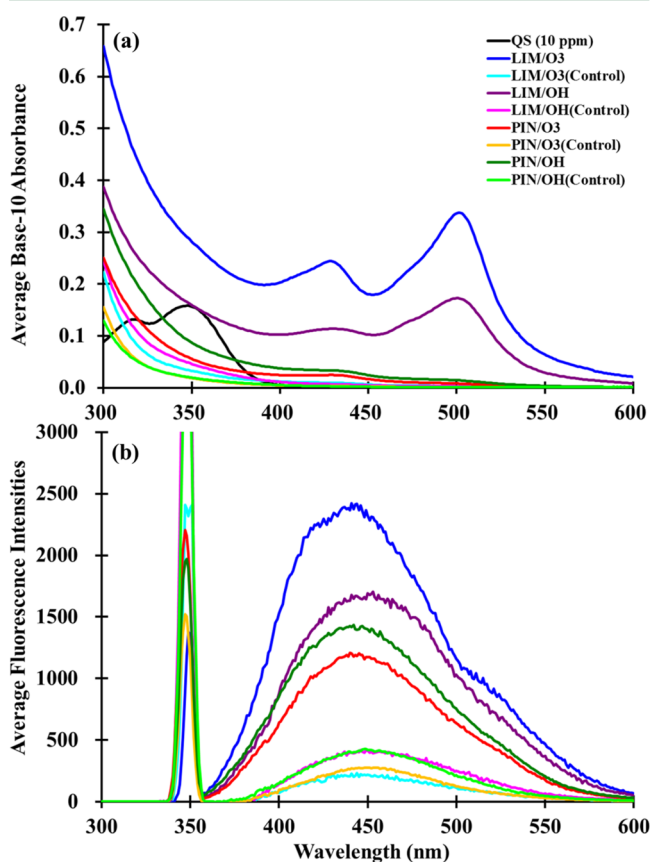


**Figure 1.** Absorption (a) and emission (b) spectra for the 1000 ppm solutions of aged and control SOA samples. The excitation wavelength for the emission spectra corresponds to the peak of the QS absorption spectrum ( $\lambda = 349$  nm, indicated by an arrow).

and this excitation wavelength was chosen for the  $QY$  measurements from the SOA solutions. The base-10 absorption coefficient for QS was determined in separate calibration measurement as described in the Supporting Information (Figure S1). For the 0.1 ppm solution used in the fluorescence measurements,  $\alpha_{QS}$  was  $0.00155 \text{ cm}^{-1}$  at 349 nm.

### 3. RESULTS AND DISCUSSION

**3.1. Absorption and Fluorescence Spectra.** The aged LIM/O<sub>3</sub> and LIM/OH exhibited a strong absorption peak at 500 nm and a weaker peak at 430 nm (Figure 1(a)), in agreement with our previous studies.<sup>24–27</sup> Absorption spectra of the aged-PIN/OH and aged-PIN/O<sub>3</sub> were considerably weaker, again consistent with our previous work.<sup>27</sup> None of the control samples developed significant absorbance in the 400–600 nm range confirming the important role of the reduced nitrogen compounds in the browning process.

Figure 1(b) shows the fluorescence spectra of the aged and control SOA samples resulting from an excitation at 349 nm. In

all cases, there was a significant Stokes shift, with the peak of the emission spectrum occurring around 450 nm. The aged-LIM/O<sub>3</sub> had the highest fluorescence intensity followed by aged-LIM/OH, aged-PIN/O<sub>3</sub>, and aged-PIN/OH. Although aged-PIN/O<sub>3</sub> or aged-PIN/OH did not visibly brown, both types of PIN SOA fluoresced with intensities comparable to those from LIM SOA.

The spectra shown in Figure 1 correspond to dilute aqueous extracts of water-soluble compounds of SOA. In contrast, the single particle fluorescence detectors record spectra from particles with relatively low water content. As the shapes of the fluorescence spectra are sensitive to the environment,<sup>1</sup> the spectra of SOA particles may look different. However, we do not expect a drastic difference in the emission peak position because of the similarity between the absorption spectra of the aged LIM/O<sub>3</sub> SOA recorded in an organic film<sup>25</sup> and in an aqueous solution.<sup>26</sup>

The excitation–emission spectra of aqueous environmental organics are commonly presented in the form of a three-dimensional excitation–emission matrix (EEM) plot,<sup>43,44</sup> wherein the emission intensity is displayed in a contour plot as a function of the excitation and emission wavelengths. Figure 2 shows the EEM plots for the four types of SOA samples examined in this work. Because of the sufficiently strong emission from the SOA, we opted not to remove the weaker Rayleigh and Raman scattering peaks from the EEM plot.<sup>43</sup> The EEM plot for LIM/O<sub>3</sub> aged with aqueous ammonium sulfate was previously reported by Bones et al.,<sup>24</sup> it was similar to the plot for LIM/O<sub>3</sub> aged with gas-phase ammonia presented in this work. The EEM plots of the aged-LIM/OH and aged-LIM/O<sub>3</sub> had a similar contour pattern, and the only difference was in their relative emission intensities. The maximum emission intensity was achieved with a 420 nm excitation (but detectable fluorescence was observed for a broad range of excitation wavelengths from 300 to 500 nm). The average Stokes shift, defined as the average difference between the peak emission wavelength and the excitation wavelength, was 55 nm for LIM SOA.

The EEM plots for the aged-PIN/O<sub>3</sub> and aged-PIN/OH were also similar to each other, as shown in Figure 2(c,d). However, compared to the aged-LIM/OH and aged-LIM/O<sub>3</sub>, the emission intensities were considerably lower and the location of the EEM peak was shifted to lower wavelength. Both aged-PIN/O<sub>3</sub> and aged-PIN/OH exhibited the maximum emission intensity when they were excited at around 325 nm, and the average Stokes shift was about 100 nm (as compared to 420 and 55 nm, respectively, for LIM SOA).

Birdwell et al.<sup>45</sup> used ratios of EEM intensities at different excitation and emission wavelengths as indicators of the type and source of the dissolved organic matter (DOM) in fog waters. The indicators used by Birdwell et al. were as follows: fluorescence index (FI) - the ratio of emission intensities at 450 and 500 nm following 370 nm excitation,<sup>46</sup> index of recent autochthonous (i.e., produced by the original source of DOM as opposed to externally produced) contribution (BIX) - the ratio of emission intensities at 380 and 430 nm following 310 nm excitation,<sup>47</sup> and humification index (HIX) - the ratio of average emission intensity in the 435–480 nm range to that in the 300–345 nm range following 254 nm excitation.<sup>48</sup> Table 1 includes all three indexes calculated for the SOA samples probed in this work, before and after aging with ammonia. In general,  $FI \sim 1.4$  is observed for terrestrially derived fulvic acids, while  $FI \sim 1.9$  corresponds to fulvic acids of microbial

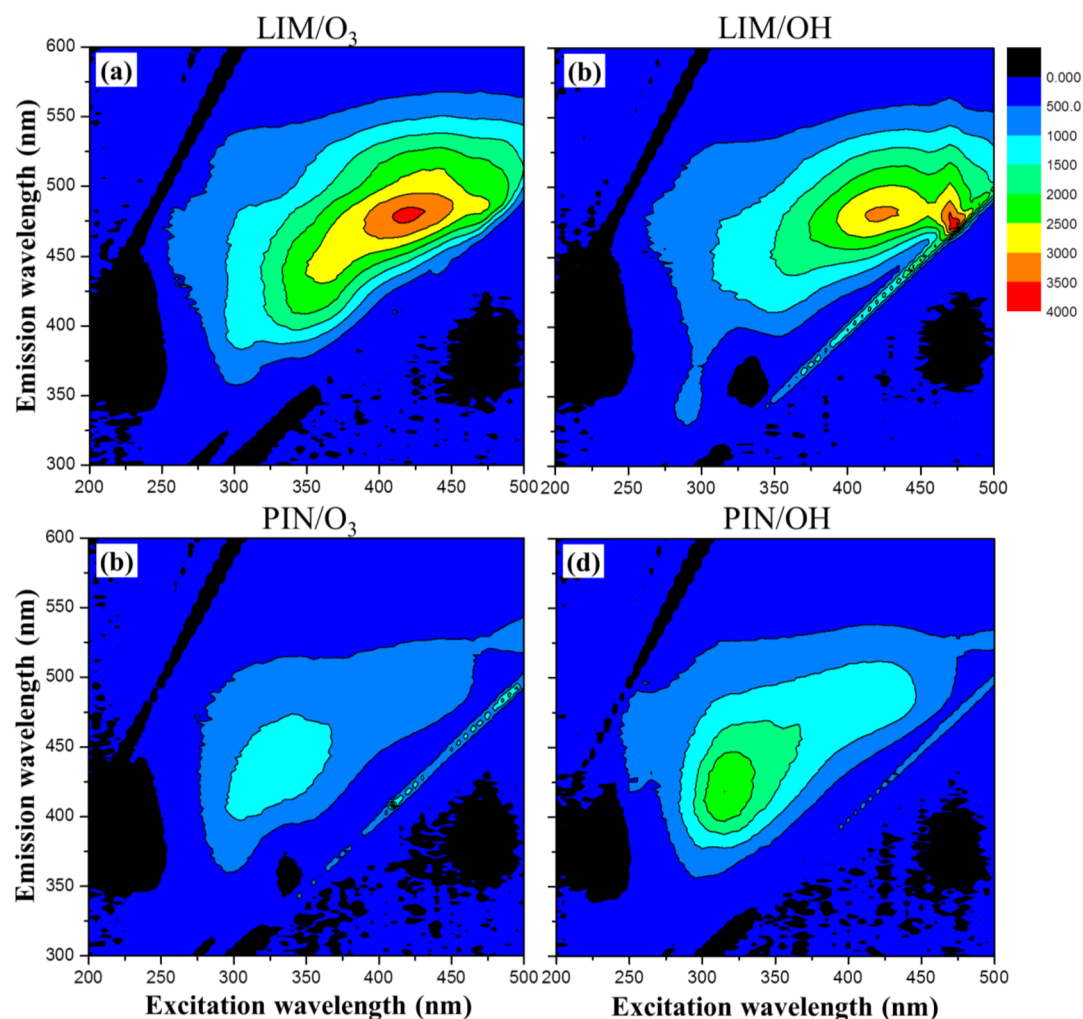


Figure 2. EEM plots for the 1000 ppm solutions of the aged SOA samples.

Table 1. Fluorescence Properties of Aged and Control SOA Samples<sup>a</sup>

| solution                | $\alpha$ (349 nm), $\text{cm}^{-1}$ | $I_{\text{area}}$ arb.units | QY (SD), % | FI (SD)    | BIX (SD)   | HIX (SD) |
|-------------------------|-------------------------------------|-----------------------------|------------|------------|------------|----------|
| QS (0.1 ppm)            | 0.00155                             | 179                         | 51         |            |            |          |
| LIM/O <sub>3</sub>      | 0.033                               | 221                         | 0.29(0.02) | 1.43(0.07) | 0.53(0.07) | 1.7(0.6) |
| aged-LIM/O <sub>3</sub> | 0.286                               | 278                         | 0.43(0.02) | 1.63(0.06) | 0.82(0.05) | 5.5(0.7) |
| LIM/OH                  | 0.046                               | 44                          | 0.42(0.07) | 1.25(0.15) | 0.40(0.01) | 1.4(0.1) |
| aged-LIM/OH             | 0.177                               | 201                         | 0.50(0.05) | 1.33(0.10) | 0.68(0.10) | 4.2(1.8) |
| PIN/O <sub>3</sub>      | 0.019                               | 260                         | 0.60(0.09) | 1.62(0.14) | 0.48(0.02) | 2.3(1.5) |
| aged-PIN/O <sub>3</sub> | 0.057                               | 133                         | 1.03(0.04) | 1.41(0.05) | 0.69(0.11) | 5.0(0.5) |
| PIN/OH                  | 0.020                               | 417                         | 0.92(0.04) | 1.86(0.09) | 0.47(0.03) | 5.0(1.9) |
| aged-PIN/OH             | 0.089                               | 163                         | 0.81(0.2)  | 1.50(0.08) | 0.57(0.01) | 6.1(1.8) |

<sup>a</sup>Measured base-10 absorption coefficients  $\alpha$  correspond to 1000 ppm (by weight) solutions of SOA and 0.1 ppm solutions of QS. The 362–600 nm integrated emission intensities correspond to the 349 nm excitation. The effective quantum yield (QY) values were calculated from eq 5. The last three columns contain the fluorescence index (FI), index of recent autochthonous contribution (BIX), and humification index (HIX) (see text for details). The numbers in parentheses correspond to one standard deviation (SD) calculated from 2–3 independent measurements.

origin.<sup>46</sup> The degree of aromaticity in fulvic acids (as assessed by the fraction of  $\text{sp}^2$  carbon) decreases from 30% to 10% when FI increases from 1.4 to 1.9.<sup>46</sup> Observed FI values of SOA fell in range of  $1.5 \pm 0.4$  corresponding to intermediate fluorescent properties relative to the terrestrial and biologic DOM. Aging increased the FI values for LIM aerosol and decreased it for PIN, but this effect was barely above the standard deviation of the measurements. According to Huguet et al., BIX  $\sim 0.6$  corresponds to DOM with low autochthonous component,

while BIX  $> 1$  is observed for DOM of biological origin.<sup>47</sup> The BIX values for the SOA samples were on average 0.6 (Table 1), consistent with their nonbiological origin. The BIX values increased upon aging for all types of SOA although the effect was, once again, relatively small. Low HIX values correspond to freshly introduced, nonhumified DOM derived from biomass, while humified DOM in mature soils exhibit considerably larger HIX values.<sup>46,48</sup> The HIX values for the fresh SOA were low, but they increased significantly upon aging with ammonia,

especially in the LIM/O<sub>3</sub> and PIN/O<sub>3</sub> cases. This increase is consistent with the reported increase in the degree of aromaticity in the SOA compounds after their reaction with ammonia.<sup>25,27</sup>

**3.2. Effective Quantum Yields.** Even though LIM and PIN SOA contain a rather complex mixture of compounds,<sup>49–53</sup> the extent of fluorescence can be quantified using an effective fluorescence quantum yield (*QY*) defined as the ratio of the number of photons emitted by the sample to the number of absorbed photons. The effective *QY* is an average of the *QY<sub>i</sub>* of individual mixture components weighted by the corresponding absorption coefficients ( $\alpha_i$ ):

$$QY = \frac{\sum \alpha_i \times QY_i}{\sum \alpha_i} \quad (1)$$

This definition is convenient because the overall fluorescence intensity from the SOA solution is directly proportional to the effective *QY*

$$I_{\text{detected}} = \gamma \times QY \times I_{\text{absorbed}} \quad (2)$$

where  $I_{\text{absorbed}}$  is the intensity of the excitation radiation absorbed by the solution,  $I_{\text{detected}}$  is the wavelength-integrated fluorescence intensity measured by the detector, and  $\gamma$  is an instrumental factor,<sup>54</sup> which depends on the transmission efficiency for the emission wavelength(s), radiant sensitivity of the detector, refractive index of the cuvette material and solution. For sufficiently dilute solutions,  $I_{\text{absorbed}}$  is directly proportional to base-10 absorption coefficient of the solution ( $\alpha$ ), the intensity of the radiation entering the cell ( $I_0$ ), and the path length ( $l$ ):<sup>54</sup>

$$I_{\text{detected}} = \gamma \times QY \times I_0 \times (1 - 10^{-\alpha l}) \\ \approx \gamma \times QY \times I_0 \times l \times \alpha \times \ln(10) \quad (3)$$

It is common to determine *QY* relative to that of a reference compound,<sup>24,42,43</sup> such as quinine sulfate (QS). The ratio of the fluorescence intensities of QS and SOA recorded under the same experimental conditions is given by eq 4:

$$\frac{I_{\text{detected}}^{\text{QS}}}{I_{\text{detected}}^{\text{SOA}}} = \frac{\gamma_{\text{QS}} \times QY_{\text{QS}} \times I_{\text{absorbed}}^{\text{QS}}}{\gamma_{\text{SOA}} \times QY_{\text{SOA}} \times I_{\text{absorbed}}^{\text{SOA}}} \approx \frac{QY_{\text{QS}} \times \alpha_{\text{QS}}}{QY_{\text{SOA}} \times \alpha_{\text{SOA}}} \quad (4)$$

The cancellation of the instrumental factors  $\gamma$  in eq 4 is an approximation because  $\gamma$  depends on the distribution of the emission wavelengths and on the refractive index of the solution. The closer are the shapes of the emission spectra of the reference compound and SOA the better this approximation holds. The difference in the refractive indexes of the SOA solution in water and QS solution in 0.05 M sulfuric acid is insignificant. With these approximations, the ratio of detected intensities becomes independent of the instrumental parameters ( $\gamma$ ,  $I_0$ , and  $l$ ), making it possible to calculate the effective *QY* of SOA from measurable quantities:

$$QY_{\text{SOA}} = QY_{\text{QS}} \times \frac{I_{\text{detected}}^{\text{SOA}} \alpha_{\text{QS}}}{I_{\text{detected}}^{\text{QS}} \alpha_{\text{SOA}}} \quad (5)$$

The concentrations of SOA or QS do not explicitly enter this equation; only the absorption coefficients from the UV–vis measurements and emission intensities from the fluorescence measurements need to be known. In this work, the excitation wavelength was 349 nm (the peak of the QS absorption

spectrum). The absorption coefficients at 349 nm were measured as described in the Experimental Section, and the emission intensities corresponded to integrated emission between 362 and 600 nm. As shown in Figure 1(b), this wavelength range contains the majority of the emission spectrum for all four types of SOA studied here. The resulting  $QY_{\text{SOA}}$  values are summarized in Table 1.

Figure 1 demonstrates that the absorption coefficients of SOA increase significantly upon aging across the UV–vis spectrum for the LIM/O<sub>3</sub> and LIM/OH and much less so for the PIN/O<sub>3</sub> and PIN/OH. However, the effective fluorescence *QY* for all the aged and control samples of SOA are of a similar order of magnitude ( $\sim 0.005$ ). This result is difficult to interpret because of the unknown (but likely very large) number of individual molecules in the SOA mixture that contribute to the absorption and emission at the 349 nm excitation wavelength. The lack of change in the effective *QY* would be consistent with a scenario, in which aging increases the concentration of all chromophores and fluorophores in SOA by the same factor (which then cancels out in eq 1), but a number of other plausible scenarios could also be envisioned. Therefore, instead of hypothesizing about the reasons for the invariance of the *QY* values with respect to the type of SOA and its aging state, we will adopt the  $QY \sim 0.005$  value as “typical” for biogenic SOA and discuss the relative fluorescence intensity from biogenic SOA and from other biological and nonbiological fluorescent particles.

Table 2 lists the main classes of fluorophores found in all types of PBAP, and their basic photophysical properties such as

**Table 2. Summary of Properties for Atmospherically-Relevant Fluorophores (From the References Listed) and for the Aged SOA Samples (This Work)<sup>a</sup>**

| fluorophore                              | $\lambda_{\text{ex}}$ [nm]<br>$\lambda_{\text{em}}$ [nm] | QY          | reference   |
|--|--|-------------|-------------|
| PBAP                                     |  |             |             |
| tryptophan (Trp)                         | 280–295<br>340–355                                       | 0.13–0.2    | 1,45        |
| tyrosine (Tyr)                           | 270–280<br>300–315                                       | 0.1–0.14    | 1,45        |
| phenylalanine (Phe)                      | 260–270<br>280–320                                       | 0.02–0.4    | 1,45        |
| nicotinamide adenine dinucleotide (NADH) | 290–370<br>390–470                                       |             | 1,45,63     |
| flavins                                  | 280–640<br>510–660                                       | $\sim 0.3$  | 1,45        |
| HULIS                                    |  |             |             |
| mid-UV HULIS                             | 240–260<br>400–460                                       | 0.003–0.022 | 45,58,64,65 |
| near-UV HULIS                            | 320–360<br>420–460                                       | 0.003–0.022 |             |
| marine HULIS                             | 290–310<br>370–410                                       | 0.02–0.05   |             |
| SOA                                      |  |             |             |
| aged LIM/O <sub>3</sub> and LIM/OH SOA   | 250–500<br>370–550                                       | 0.004       | this work   |
| aged PIN/O <sub>3</sub> and PIN/OH SOA   | 280–470<br>350–520                                       | 0.008       | this work   |

<sup>a</sup>The table specifies the approximate range of the excitation ( $\lambda_{\text{ex}}$ ) and emission ( $\lambda_{\text{em}}$ ) wavelengths and the fluorescence quantum yield (*QY*). The *QY* for NADH is not listed because it is highly sensitive to the intracellular conditions.

the typical excitation and the emission wavelength ranges and the fluorescence  $QY$  values. The most important fluorophores in PBAP include amino acids with aromatic side-chains such as tryptophan, tyrosine, and phenylalanine, certain coenzymes such as nicotinamide adenine dinucleotide (NADH), and flavins such as riboflavin.<sup>1</sup> There are many other classes of fluorophores in PBAP that occur in specific organisms, such as chitin in fungi, cellulose in plants, sporopollenin in pollen and spores, etc. They are not included in Table 2, but a comprehensive list of the relevant PBAP fluorophores can be found in Table 1 of ref 1. One of the most important nonbiological fluorescent aerosols included in Table 2 is HULIS, which stands for "HUMic-Like Substances".<sup>1</sup> Atmospheric HULIS is a complex mixture of heterogeneous compounds originating from multiple sources such as primary emission by biomass burning and secondary atmospheric oxidation of products of lignin pyrolysis.<sup>55–58</sup> Environmental researchers distinguish three types of HULIS by the regions of the EEM plot in which their emission appears.<sup>42,43,45,59,60</sup> For example, dissolved organic matter of marine origin tends to fluorescence the strongest when excited around 300 nm, with the emission appearing predominantly between 370 and 410 nm. To facilitate the discussion, Figure 3 provides a graphical representation of where different fluorophores appear in EEM plots; for simplicity all three types of HULIS have been combined together in Figure 3.

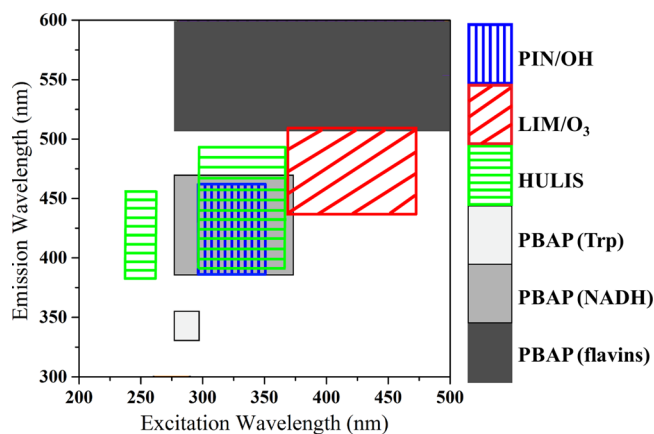


**Figure 3.** Approximate locations of the highest emission intensities in the EEM plots for HULIS, PBAP, and aged SOA. The dimensions of the rectangles correspond to the fwhm of the emission and excitation spectra. PIN and LIM data are from this work, while HULIS and PBAP are from references listed in Table 2. The PIN and LIM EEM regions overlap to some extent with regions corresponding to NADH and PBAP.

According to Figure 2, the aged-PIN/O<sub>3</sub> and PIN/OH fluoresce the strongest in the window of  $\lambda_{\text{excitation}} = 320 \pm 25$  nm and  $\lambda_{\text{emission}} = 425 \pm 38$  nm, where the center values correspond to the peak intensity and the wavelength span corresponds to the fwhm along the corresponding cut through the EEM data. As shown in Table 2 and Figure 3, this range overlaps with the fluorescence from NADH and with the near-UV peak of HULIS. The aged-LIM/O<sub>3</sub> and LIM/OH have the maximum emission at  $\lambda_{\text{excitation}} = 420 \pm 50$  nm and  $\lambda_{\text{emission}} = 475 \pm 38$  nm. Figure 3 suggests that aged-LIM can be distinguished from the PBAP and HULIS on an EEM plot. One has to keep in mind, however, that the single particle fluorescence detectors do not record the entire EEM plot.

They operate at a single excitation wavelength (or two separate excitation wavelengths), most commonly in the range of 280–370 nm, and record either integrated or wavelength resolved emission. Under these excitation conditions, all four types of SOA would have some level of spectral interference with PBAP fluorescence.

Is this interference significant? To answer this question we compare the expected intensity of fluorescence from a PBAP particle and from an SOA particle of the same size. It is straightforward to show that the relative emission intensity from these particles can be predicted using eq 6

$$\text{Ratio} = \frac{I_{\text{detected}}^{\text{PBAP}}}{I_{\text{detected}}^{\text{SOA}}} = \frac{\alpha_{\text{PBAP}}(\lambda_{\text{ex}}) \times QY_{\text{PBAP}}}{\alpha_{\text{SOA}}(\lambda_{\text{ex}}) \times QY_{\text{SOA}}} \quad (6)$$

where  $QY$  is the effective quantum yield as defined in eq 1, and  $\alpha$  represents some measure of the total absorption of the excitation wavelength by the particle (we will use the absorption coefficient of a solution containing a certain mass concentration of particles, dispersed down to the level of individual molecular components). Use of the absorption coefficients and quantum yields for a dilute aqueous solution is approximate because they may change in a dry particle, but it is convenient because data from Table 1 can be directly inserted in eq 6.

Just like SOA, PBAP is composed of a complex mixture of fluorescent and nonfluorescent constituents. We will consider a highly oversimplified case, in which PBAP fluorescence is dominated by a single compound, amino acid tryptophan. Tryptophan typically accounts for ~1% of protein content<sup>61</sup> but it is responsible for about 90% of fluorescence from PBAP.<sup>1</sup> According to Schneider et al.,<sup>62</sup> the overall dry mass fraction of protein in PBAP ranges from 10 to 70%. Taking the lower limit, a 1000 ppm solution of PBAP could contain  $10^{-3}$  g/L ( $5 \mu\text{M}$ ) of tryptophan. Under the optimal excitation conditions for tryptophan, at  $\lambda_{\text{excitation}} = 280$  nm, its molar extinction coefficient is  $\epsilon_{\text{trp}} = 5500 \text{ M}^{-1} \text{ cm}^{-1}$ ,<sup>61</sup> and the  $QY \sim 0.2$  (Table 2). If we compare this to the fluorescence from SOA under its optimal conditions ( $\alpha_{\text{SOA}} = 0.3 \text{ cm}^{-1}$ ;  $QY_{\text{SOA}} = 0.005$ ), we will get a ratio of ~4 from eq 6. The optimal conditions for the excitation of SOA and tryptophan are not the same, but our goal is to compare the orders of magnitude of the maximum emission intensity from an SOA particle and from a PBAP particle. Even though this is an approximate calculation that neglects other fluorophores, fluorescence quenching in the particle, and other factors, it demonstrates that the intensity of fluorescence observed from an SOA particle could be comparable to that from a PBAP. The higher frequency of detecting aged terpenes during field studies on fluorescence particles further supports the importance of this finding.<sup>22</sup>

## ■ ASSOCIATED CONTENT

### 📄 Supporting Information

Figure S1. This material is available free of charge via the Internet at <http://pubs.acs.org>.

## ■ AUTHOR INFORMATION

### Corresponding Author

\*Phone: 949-824-1262. E-mail: [nizkorod@uci.edu](mailto:nizkorod@uci.edu).

### Notes

The authors declare no competing financial interest.

## ACKNOWLEDGMENTS

The UCI group acknowledges support by the NSF grants AGS-1227579 (H.J.L.) and CHEM-0909227 (S.A.N.). The PNNL group acknowledges support from the Chemical Sciences Division (J.L.), Office of Basic Energy Sciences of the U.S. DOE, and Laboratory Directed Research and Development program (A.L.) of the W.R. Wiley Environmental Molecular Sciences Laboratory (EMSL) - a national scientific user facility located at PNNL, and sponsored by the Office of Biological and Environmental Research of the U.S. PNNL is operated for US DOE by Battelle Memorial Institute under Contract No. DE-AC06-76RL0 1830.

## REFERENCES

- (1) Pöhlker, C.; Huffman, J. A.; Pöschl, U. Autofluorescence of atmospheric bioaerosols – fluorescent biomolecules and potential interferences. *Atmos. Meas. Tech.* **2012**, *5*, 37–71.
- (2) Hallar, A. G.; Chirokova, G.; McCubbin, I.; Painter, T. H.; Wiedinmyer, C.; Dodson, C. Atmospheric bioaerosols transported via dust storms in the western United States. *Geophys. Res. Lett.* **2011**, *38*, L17801 DOI: 17810.11029/12011GL048166.
- (3) Douwes, J.; Thorne, P.; Pearce, N.; Heederik, D. Bioaerosol health effects and exposure assessment: progress and prospects. *Ann. Occup. Hyg.* **2003**, *47*, 187–200.
- (4) Pratt, K. A.; DeMott, P. J.; French, J. R.; Wang, Z.; Westphal, D. L.; Heymsfield, A. J.; Twohy, C. H.; Prenni, A. J.; Prather, K. A. In situ detection of biological particles in cloud ice-crystals. *Nat. Geosci.* **2009**, *2*, 398–401.
- (5) Poeschl, U.; Martin, S. T.; Sinha, B.; Chen, Q.; Gunthe, S. S.; Huffman, J. A.; Borrmann, S.; Farmer, D. K.; Garland, R. M.; Helas, G.; Jimenez, J. L.; King, S. M.; Manzi, A.; Mikhailov, E.; Pauliquevis, T.; Petters, M. D.; Prenni, A. J.; Roldin, P.; Rose, D.; Schneider, J.; Su, H.; Zorn, S. R.; Artaxo, P.; Andreae, M. O. Rainforest aerosols as biogenic nuclei of clouds and precipitation in the Amazon. *Science* **2010**, *329*, 1513–1516.
- (6) DeMott, P. J.; Prenni, A. J. New directions: need for defining the numbers and sources of biological aerosols acting as ice nuclei. *Atmos. Environ.* **2010**, *44*, 1944–1945.
- (7) Hill, S. C.; Pinnick, R. G.; Niles, S.; Pan, Y.-L.; Holler, S.; Chang, R. K.; Bottiger, J.; Chen, B. T.; Orr, C.-S.; Feather, G. Real-time measurement of fluorescence spectra from single airborne biological particles. *Anal. Chem. Technol.* **1999**, *3*, 221–239.
- (8) Ammor, M. Recent advances in the use of intrinsic fluorescence for bacterial identification and characterization. *J. Fluoresc.* **2007**, *17*, 455–459.
- (9) Pinnick, R. G.; Hill, S. C.; Pan, Y.-L.; Chang, R. K. Fluorescence spectra of atmospheric aerosol at Adelphi, Maryland, USA: measurement and classification of single particles containing organic carbon. *Atmos. Environ.* **2004**, *38*, 1657–1672.
- (10) Huffman, J. A.; Treutlein, B.; Pöschl, U. Fluorescent biological aerosol particle concentrations and size distributions measured with an ultraviolet aerodynamic particle sizer (UV-APS) in Central Europe. *Atmos. Chem. Phys.* **2010**, *10*, 3215–3233.
- (11) Pan, Y.-L.; Chang, R. K.; Hill, S. C.; Pinnick, R. G. Using single-particle fluorescence to detect bioaerosols. *Opt. Photonics News* **2008**, *19*, 29–33.
- (12) Pan, Y.-L.; Hill, S. C.; Pinnick, R. G.; Huang, H.; Bottiger, J. R.; Chang, R. K. Fluorescence spectra of atmospheric aerosol particles measured using one or two excitation wavelengths: comparison of classification schemes employing different emission and scattering results. *Opt. Express* **2010**, *18*, 12436–12457.
- (13) Pan, Y.-L.; Pinnick, R. G.; Hill, S. C.; Rosen, J. M.; Chang, R. K. Single-particle laser-induced-fluorescence spectra of biological and other organic-carbon aerosols in the atmosphere: measurements at New Haven, Connecticut, and Las Cruces, New Mexico. *J. Geophys. Res.* **2007**, *112*, D24S19 DOI: 10.1029/2007JD008741.
- (14) Kaye, P.; Stanley, W. R.; Hirst, E.; Foot, E. V.; Baxter, K. L.; Barrington, S. J. Single particle multichannel bio-aerosol fluorescence sensor. *Opt. Express* **2005**, *13*, 3583–3593.
- (15) Gabey, A. M.; Stanley, W. R.; Gallagher, M. W.; Kaye, P. H. The fluorescence properties of aerosol larger than 0.8  $\mu\text{m}$  in urban and tropical rainforest locations. *Atmos. Chem. Phys.* **2011**, *11*, 5491–5504.
- (16) Hill, S. C.; Pinnick, R. G.; Nachman, P.; Chen, G.; Chang, R. K.; Mayo, M. W.; Fernandez, G. L. Aerosol-fluorescence spectrum analyzer: real-time measurement of emission spectra of airborne biological particles. *Appl. Opt.* **1995**, *34*, 7149–7155.
- (17) Hirst, E.; Kaye, P. H.; Foot, V. E.; Clark, J. M.; Withers, P. B. An instrument for the simultaneous acquisition of size, shape, and spectral fluorescence data from single aerosol particles. *Proc. SPIE-Int. Soc. Opt. Eng.* **2004**, *5617*, 416–423.
- (18) Jonsson, P.; Kullander, F.; Vahlberg, C.; Jelger, P.; Tiihonen, M.; Waesterby, P.; Tjaernhage, T.; Lindgren, M. Spectral detection of ultraviolet laser induced fluorescence from individual bio-aerosol particles. *Proc. SPIE-Int. Soc. Opt. Eng.* **2006**, *6398*, 63980F/63981–63980F/63912.
- (19) Pinnick, R. G.; Hill, S. C.; Nachman, P.; Videen, G.; Chen, G.; Chang, R. K. Aerosol fluorescence spectrum analyzer for rapid measurement of single micrometer-sized airborne biological particles. *Aerosol Sci. Technol.* **1998**, *28*, 95–104.
- (20) Agranovski, V.; Ristovski, Z.; Hargreaves, M.; Blackall, P. J.; Morawska, L. Real-time measurement of bacterial aerosols with the UVAPS: performance evaluation. *J. Aerosol Sci.* **2003**, *34*, 301–317.
- (21) You, Y.; Renbaum-Wolff, L.; Carreras-Sospedra, M.; Hanna, S. J.; Hiranuma, N.; Kamal, S.; Smith, M. L.; Zhang, X.; Weber, R. J.; Shilling, J. E.; Dabdub, D.; Martin, S. T.; Bertram, A. K. Images reveal that atmospheric particles can undergo liquid–liquid phase separations. *Proc. Natl. Acad. Sci.* **2012**, *109*, 13188–13193.
- (22) Pinnick, R. G.; Fernandez, E.; Rosen, J. M.; Hill, S. C.; Wang, Y.; Pan, Y. L. Fluorescence spectra and elastic scattering characteristics of atmospheric aerosol in Las Cruces, New Mexico, USA: variability of concentrations and possible constituents and sources of particles in various spectral clusters. *Atmos. Environ.* **2013**, *65*, 195–204.
- (23) Bond, T.; Bergstrom, R. Light absorption by carbonaceous particles: an investigative review. *Aerosol Sci. Technol.* **2006**, *40*, 27–67.
- (24) Bones, D. L.; Henricksen, D. K.; Mang, S. A.; Gonsior, M.; Bateman, A. P.; Nguyen, T. B.; Cooper, W. J.; Nizkorodov, S. A. Appearance of strong absorbers and fluorophores in limonene-O<sub>3</sub> secondary organic aerosol due to NH<sub>4</sub><sup>+</sup>-mediated chemical aging over long time scales. *J. Geophys. Res.* **2010**, *115*, D05203 DOI: 05210.01029/02009JD012864.
- (25) Laskin, J.; Laskin, A.; Roach, P. J.; Slysz, G. W.; Anderson, G. A.; Nizkorodov, S. A.; Bones, D. L.; Nguyen, L. Q. High-resolution desorption electrospray ionization mass spectrometry for chemical characterization of organic aerosols. *Anal. Chem.* **2010**, *82*, 2048–2058.
- (26) Nguyen, T. B.; Lee, P. B.; Updyke, K. M.; Bones, D. L.; Laskin, J.; Laskin, A.; Nizkorodov, S. A. Formation of nitrogen- and sulfur-containing light-absorbing compounds accelerated by evaporation of water from secondary organic aerosols. *J. Geophys. Res.* **2012**, *117*, D01207 DOI: 01210.01029/02011JD016944.
- (27) Updyke, K. M.; Nguyen, T. B.; Nizkorodov, S. A. Formation of brown carbon via reactions of ammonia with secondary organic aerosols from biogenic and anthropogenic precursors. *Atmos. Environ.* **2012**, *63*, 22–31.
- (28) De Haan, D. O.; Corrigan, A. L.; Tolbert, M. A.; Jimenez, J. L.; Wood, S. E.; Turley, J. J. Secondary organic aerosol formation by self-reactions of methylglyoxal and glyoxal in evaporating droplets. *Environ. Sci. Technol.* **2009**, *43*, 8184–8190.
- (29) De Haan, D. O.; Corrigan, A. L.; Smith, K. W.; Stroik, D. R.; Turley, J. J.; Lee, F. E.; Tolbert, M. A.; Jimenez, J. L.; Cordova, K. E.; Ferrell, G. R. Secondary organic aerosol-forming reactions of glyoxal with amino acids. *Environ. Sci. Technol.* **2009**, *43*, 2818–2824.
- (30) Zarzana, K.; De Haan, D.; Freedman, M.; Hasenkopf, C.; Tolbert, M. Optical properties of the products of  $\alpha$ -dicarbonyl and

amine reactions in simulated cloud droplets. *Environ. Sci. Technol.* **2012**, *46*, 4845–4851.

(31) Shapiro, E. L.; Szprengiel, J.; Sareen, N.; Jen, C. N.; Giordano, M. R.; McNeill, V. F. Light-absorbing secondary organic material formed by glyoxal in aqueous aerosol mimics. *Atmos. Chem. Phys.* **2009**, *9*, 2289–2300.

(32) Galloway, M. M.; Chhabra, P. S.; Chan, A. W. H.; Surratt, J. D.; Flagan, R. C.; Seinfeld, J. H.; Keutsch, F. N. Glyoxal uptake on ammonium sulphate seed aerosol: reaction products and reversibility of uptake under dark and irradiated conditions. *Atmos. Chem. Phys.* **2009**, *9*, 3331–3345.

(33) Yu, G.; Bayer, A. R.; Galloway, M. M.; Korshavn, K. J.; Fry, C. G.; Keutsch, F. N. Glyoxal in aqueous ammonium sulfate solutions: products, kinetics and hydration effects. *Environ. Sci. Technol.* **2011**, *45*, 6336–6342.

(34) Trainic, M.; Abo Riziq, A.; Lavi, A.; Flores, J. M.; Rudich, Y. The optical, physical and chemical properties of the products of glyoxal uptake on ammonium sulfate seed aerosols. *Atmos. Chem. Phys.* **2011**, *11*, 9697–9707.

(35) Sareen, N.; Schwier, A. N.; Shapiro, E. L.; Mitroo, D.; McNeill, V. F. Secondary organic material formed by methylglyoxal in aqueous aerosol mimics. *Atmos. Chem. Phys.* **2010**, *10*, 997–1016.

(36) Noziere, B.; Dziedzic, P.; Cordova, A. Formation of secondary light-absorbing "fulvic-like" oligomers: a common process in aqueous and ionic atmospheric particles? *Geophys. Res. Lett.* **2007**, *34*, L21812 DOI: 21810.21029/22007GL031300.

(37) Noziere, B.; Dziedzic, P.; Cordova, A. Inorganic ammonium salts and carbonate salts are efficient catalysts for aldol condensation in atmospheric aerosols. *Phys. Chem. Chem. Phys.* **2010**, *12*, 3864–3872.

(38) Andreae, M. O.; Gelencser, A. Black carbon or brown carbon? The nature of light-absorbing carbonaceous aerosols. *Atmos. Chem. Phys.* **2006**, *6*, 3131–3148.

(39) Nguyen, T. B.; Laskin, J.; Laskin, A.; Nizkorodov, S. A. Nitrogen-containing organic compounds and oligomers in secondary organic aerosol formed by photooxidation of isoprene. *Environ. Sci. Technol.* **2011**, *45*, 6908–6918.

(40) Clegg, S. L.; Brimblecombe, P.; Wexler, A. S. Thermodynamic model of the system  $\text{H}^+\text{-NH}_4^+\text{-Na}^+\text{-SO}_4^{2-}\text{-NO}_3^-\text{-Cl}^-\text{-H}_2\text{O}$  at tropospheric temperatures. *J. Phys. Chem. A* **1998**, *102*, 2137–2154.

(41) Montalti, M.; Credi, A.; Prodi, L.; Gandolfi, M. T. Luminescence Spectroscopy Measurements. In *Handbook of Photochemistry*, 3rd ed.; CRC Press Taylor & Francis Group: Boca Raton, FL, 2006; p 574.

(42) Zepp, R. G.; Baughman, G. L.; Schlotzhauer, P. F. Comparison of photochemical behavior of various humic substances in water: II. Photosensitized oxygenations. *Chemosphere* **1981**, *10*, 119–126.

(43) Zepp, R. G.; Sheldon, W. M.; Moran, M. A. Dissolved organic fluorophores in southeastern US coastal waters: correction method for eliminating Rayleigh and Raman scattering peaks in excitation-emission matrices. *Mar. Chem.* **2004**, *89*, 15–36.

(44) Duarte, R. M. B. O.; Pio, C. A.; Duarte, A. C. Synchronous scan and excitation-emission matrix fluorescence spectroscopy of water-soluble organic compounds in atmospheric aerosols. *J. Atmos. Chem.* **2004**, *48*, 157–171.

(45) Birdwell, J. E.; Valsaraj, K. T. Characterization of dissolved organic matter in fogwater by excitation-emission matrix fluorescence spectroscopy. *Atmos. Environ.* **2010**, *44*, 3246–3253.

(46) McKnight, D. M.; Boyer, E. W.; Westerhoff, P. K.; Doran, P. T.; Thomas, K.; Andersen, D. T. Spectrofluorometric characterization of dissolved organic matter for indication of precursor organic material and aromaticity. *Limnol. Oceanogr.* **2001**, *46*, 38–48.

(47) Huguet, A.; Vacher, L.; Relexans, S.; Saubusse, S.; Froidefond, J. M.; Parlanti, E. Properties of fluorescent dissolved organic matter in the Gironde Estuary. *Org. Geochem.* **2009**, *40*, 706–719.

(48) Zsolnay, A.; Baigar, E.; Jimenez, M.; Steinweg, B.; Saccomandi, F. Differentiating with fluorescence spectroscopy the sources of dissolved organic matter in soils subjected to drying. *Chemosphere* **1999**, *38*, 45–50.

(49) Bateman, A. P.; Nizkorodov, S. A.; Laskin, J.; Laskin, A. Time-resolved molecular characterization of limonene/ozone aerosol using high-resolution electrospray ionization mass spectrometry. *Phys. Chem. Chem. Phys.* **2009**, *11*, 7931–7942.

(50) Walser, M. L.; Desyaterik, Y.; Laskin, J.; Laskin, A.; Nizkorodov, S. A. High-resolution mass spectrometric analysis of secondary organic aerosol produced by ozonation of limonene. *Phys. Chem. Chem. Phys.* **2008**, *10*, 1009–1022.

(51) Reinhardt, A.; Emmenegger, C.; Gerrits, B.; Panse, C.; Dommen, J.; Baltensperger, U.; Zenobi, R.; Kalberer, M. Ultrahigh mass resolution and accurate mass measurements as a tool to characterize oligomers in secondary organic aerosols. *Anal. Chem.* **2007**, *79*, 4074–4082.

(52) Heaton, K. J.; Dreyfus, M. A.; Wang, S.; Johnston, M. V. Oligomers in the early stage of biogenic secondary organic aerosol formation and growth. *Environ. Sci. Technol.* **2007**, *41*, 6129–6136.

(53) Heaton, K. J.; Sleighter, R. L.; Hatcher, P. G.; Hall, W. A. L.; Johnston, M. V. Composition domains in monoterpene secondary organic aerosol. *Environ. Sci. Technol.* **2009**, *43*, 7797–7802.

(54) Strobel, H. A.; Heineman, W. R. *Chemical Instrumentation: A Systematic Approach*; John Wiley & Sons, 1989.

(55) Hoffer, A.; Gelencsér, A.; Guyon, P.; Kiss, G.; Schmid, O.; Frank, G. P.; Artaxo, P.; Andreae, M. O. Optical properties of humic-like substances (HULIS) in biomass-burning aerosols. *Atmos. Chem. Phys.* **2006**, *6*, 3563–3570.

(56) Limbeck, A.; Kulmala, M.; Puxbaum, H. Secondary organic aerosol formation in the atmosphere via heterogeneous reaction of gaseous isoprene on acidic particles. *Geophys. Res. Lett.* **2003**, *30*, 1996.

(57) Reid, J. S.; Koppmann, R.; Eck, T. F.; Eleuterio, D. P. A review of biomass burning emissions part II: intensive physical properties of biomass burning particles. *Atmos. Chem. Phys.* **2005**, *5*, 799–825.

(58) Graber, E. R.; Rudich, Y. Atmospheric HULIS: how humic-like are they? A comprehensive and critical review. *Atmos. Chem. Phys.* **2006**, *6*, 729–753.

(59) Kiss, G.; Tombacz, E.; Varga, B.; Alsberg, T.; Persson, L. Estimation of the average molecular weight of humic-like substances isolated from fine atmospheric aerosol. *Atmos. Environ.* **2003**, *37*, 3783–3794.

(60) Le Coupanec, F.; Morin, D.; Sire, O.; Peron, J. J. Characterization of dissolved organic matter (DOM) in landfill leachates using fluorescence excitation-emission matrix. *Environ. Technol.* **2000**, *21*, 515–524.

(61) Pace, C.; Vajdos, F.; Fee, L.; Grimsley, G.; Gray, T. How to measure and predict the molar absorption coefficient of a protein. *Protein Sci.* **1995**, *4*, 2411–2423.

(62) Schneider, J.; Freutel, F.; Zorn, S. R.; Chen, Q.; Farmer, D. K.; Jimenez, J. L.; Martin, S. T.; Artaxo, P.; Wiedensohler, A.; Borrmann, S. Mass-spectrometric identification of primary biological particle markers and application to pristine submicron aerosol measurements in Amazonia. *Atmos. Chem. Phys.* **2011**, *11*, 11415–11429.

(63) Cantor, C. R.; Schimmel, P. R. *Fluorescence Spectroscopy. In Biophysical Chemistry, Part 2: Techniques for the Study of Biological Structure and Function*, 11th ed.; McCombs, L. W., Ed.; W. H. Freeman and Company: United States, 1998; p 444.

(64) Gosteva, O. Y.; Izosimov, A. A.; Patsaeva, S. V.; Yuzhakov, V. I.; Yakimenko, O. S. Fluorescence of aqueous solutions of commercial humic products. *J. Appl. Spectrosc.* **2012**, *78*.

(65) Hudson, N.; Baker, A.; Reynolds, D. Fluorescence analysis of dissolved organic matter in natural, waste and polluted waters—a review. *River Res. Appl.* **2007**, *23*, 631–649.